GEOPHYSICAL RESEARCH LETTERS, VOL. 40, 5652–5657, doi:10.1002/2013GL057401, 2013

Finite frequency whole mantle *P* wave tomography: Improvement of subducted slab images

Masayuki Obayashi,[1] Junko Yoshimitsu,[1] Guust Nolet,[2] Yoshio Fukao,[1] Hajime Shiobara,[3] Hiroko Sugioka,[1] Hiroki Miyamachi,[4] and Yuan Gao[5]

Received 23 July 2013; revised 14 October 2013; accepted 17 October 2013; published 13 November 2013.

[1] We present a new whole mantle *P* wave tomographic model GAP_P4. We used two data groups; short-period data of more than 10 million picked-up onset times and long-period data of more than 20 thousand differential travel times measured by waveform cross correlation. Finite frequency kernels were calculated at the corresponding frequency bands for both long- and short-period data. With respect to an earlier model GAP_P2, we find important improvements especially in the transition zone and uppermost lower mantle beneath the South China Sea and the southern Philippine Sea owing to broadband ocean bottom seismometers (BBOBSs) deployed in the western Pacific Ocean where station coverage is poor. This new model is different from a model in which the full data set is interpreted with classical ray theory. BBOBS observations should be more useful to sharpen images of subducted slabs than expected from simple raypath coverage arguments.
Citation: Obayashi, M., J. Yoshimitsu, G. Nolet, Y. Fukao, H. Shiobara, H. Sugioka, H. Miyamachi, and Y. Gao (2013), Finite frequency whole mantle *P* wave tomography: Improvement of subducted slab images, *Geophys. Res. Lett.*, *40*, 5652–5657, doi:10.1002/2013GL057401.

1. Introduction

[2] *P* wave travel time tomography has been an efficient technique to investigate the complex morphology of subducting slabs [e.g., *van der Hilst et al*., 1991, 1997; *Fukao et al*., 1992, 2001, 2009; *Bijwaard et al*., 1998; *Kennett et al*., 1998; *Boschi and Dziewonski*, 1999; *Li et al*., 2008; *Obayashi et al*., 2009; *Simmons et al*., 2012]. The resolution of the slab images, however, strongly depends on the distributions of hypocenters and stations. One way to obtain a better resolution is to increase seismic observations in the areas of poor station coverage, e.g., by deployment of broadband ocean bottom seismometers (BBOBSs) on deep seafloors [e.g., *Shiobara et al*., 2009], where the high-background noise level at periods less than 5 s makes it in general difficult to measure the onset time of phase arrivals on the BBOBS (or ordinary OBS) records for teleseismic events. Instead, we usually measure relative travel times between two different stations by a waveform cross-correlation method at frequencies around 0.1 Hz or less [*Toomey et al*., 1998; *Tanaka et al*., 2009]. The sensitivity kernel in this frequency range is quite different from the kernel based on the ray theory [*Hung et al*., 2000; *Liu and Tromp*, 2008]. As the finite frequency tomography is effective in the region of poor raypath coverage, it has been of great benefit to investigate plumelike slow anomalies beneath hot spots, especially in the ocean [*Monetelli et al*., 2004]. In this paper we update our *P* wave tomographic model GAP_P2 [*Obayashi et al*., 2009] by increasing the first arrival time data from about 7 million to about 11 million, incorporating extensive data sets of differential travel times measured on broadband seismograms retrieved mainly from deep seafloors and oceanic islands, and take the finite frequency effect into account for all the short-period and broadband data. Regional finite frequency tomography has been successfully attempted to sharpen the remnant slab images of the Farallon plate beneath North America, where the densely spaced USArray (http://www.usarray.org/) is in operation [*Sigloch et al*., 2008; *Sigloch*, 2011; *Sigloch and Mihalynuk*, 2013] and those of the Tethys plate beneath Tibet [*Hung et al*., 2011]. In many currently active subduction zones, on the other hand, a large amount of short-period arrival time data is already available while the relevant broadband data are limited. With the exception of the Juan de Fuca slab in the North America model of *Sigloch et al*. [2008], there have been no reports of improving images of currently subducting slabs by finite frequency tomography. The purpose of the present paper is to present a new *P* wave tomographic model focused on subduction zone structures and to discuss how important the finite frequency correction is to improve subducting slab images.

2. Data and Method

[3] We used two groups of travel time data in terms of wave period. One is short-period (empirically ~1 s) data corresponding to manually picked onset times of the first arrivals. The other is long-period (around 10 s) data corresponding to relative travel times of *P* waves between two different stations and PP–P differential travel times. The first group consists of ~11.3 million arrival times reported to the International Seismological Centre (ISC) in the period of 1964 to 2008 and ~60,000 onset times visually picked on the broadband seismograms mainly from the Ocean Hemisphere Project

Additional supporting information may be found in the online version of this article.

[1]Institute for Research on Earth Evolution, Japan Agency for Marine-Earth Science and Technology, Kanagawa, Japan.
[2]Geosciences Azur, Sophia Antipolis, France.
[3]Earthquake Research Institute, University of Tokyo, Tokyo, Japan.
[4]Graduate School of Science and Engineering, Kagoshima University, Kagoshima, Japan.
[5]Institute of Earthquake Science, China Earthquake Administration, Beijing, China.

Corresponding author: M. Obayashi, Institute for Research on Earth Evolution, Japan Agency for Marine-Earth Science and Technology, 2-15 Natsushima, Yokosuka, Kanagawa 237-0061, Japan. (obayashi@jamstec.go.jp)

0094-8276/13/10.1002/2013GL057401

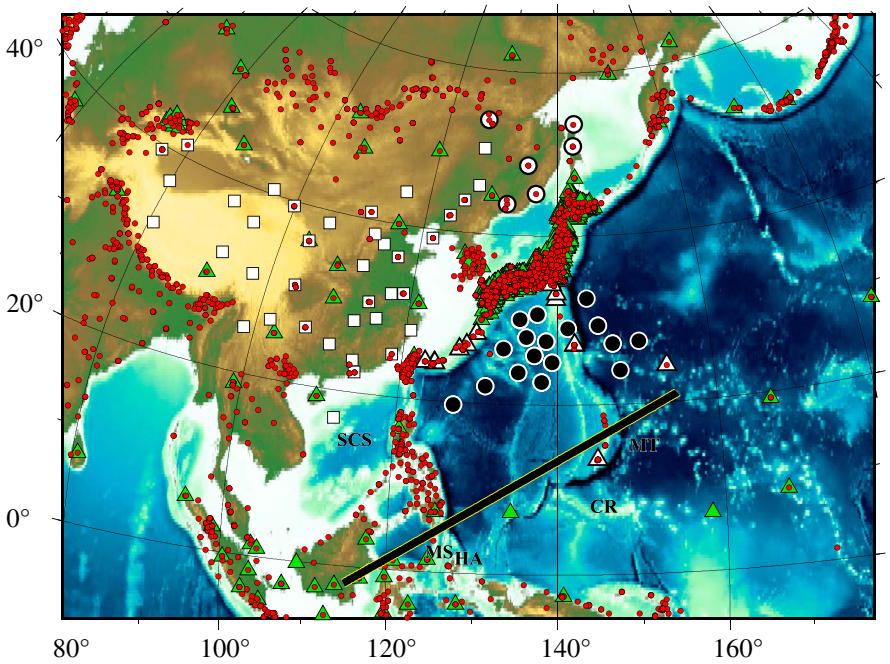

Figure 1. Stations in the region of interest. Circles show broadband seismometer stations deployed by the "Stagnant Slab Project"; closed circles for the BBOBSs in the western Pacific and open circles for stations from the Russian Far East. Squares (NSNC) and triangles (OHP, F-net, IRIS) are broadband seismometer stations used for manual picking of first arrivals. Open triangles show broadband stations used for differential time measurement by waveform cross correlation. Red dots indicate ISC stations. The thick line is the one along which the tomographic cross sections are taken. SCS = South China Sea, MT = Mariana Trench, MS = Molucca Sea, HA = Halmahera Arc, and CR = Caroline Ridge.

(OHP) network (http://www.jamstec.go.jp/pacific21/ or http://ohpdmc.eri.u-tokyo.ac.jp/) in the western Pacific, the National Seismic Network of China network (NSNC, squares in Figure 1), the F-net [*Okada et al*., 2004] in Japan, and the Skippy network in Australia (http://www.ga.gov.au/meta/ANZCW0703003617.html). The second group includes about 15,000 PP–P differential time data from the Incorporated Research Institutions for Seismology (IRIS) broadband seismic network (http://www.iris.edu/) with the correction for time shifts due to the crustal reverberations at the PP bounce points [*Obayashi et al*., 2004]. These PP–P differential times were used to construct our previous model GAP_P2 [*Obayashi et al*., 2009]. The second group also includes ~4300 relative travel time data from the western Pacific BBOBS array and ~900 relative travel time data from the Russian Far East broadband seismic array. These two broadband seismic arrays were deployed from 2005 to 2007 along with the Japanese 5 year project "Stagnant Slab Project" that started in 2004 [*Shiobara et al*., 2009; *Miyamachi et al*., 2009]. The locations of the BBOBS stations are shown by closed circles in Figure 1. These BBOBS data have been used for surface wave tomography [*Isse et al*., 2009, 2010], receiver function analyses [*Suetsugu et al*., 2010], and seismic anisotropy studies [*Isse et al*., 2010]. Our effort of extracting *P* wave arrival time information from the raw records resulted in only ~1200 readings because of the high-seafloor noise levels at periods around 5 s due to microseisms and at periods above 50 s due to ocean infragravity waves. The seafloor acceleration noise level in general takes its minimum in the period range in between, where it is as low as that in seismically quiet continents [*Webb*, 1998; *Sugioka et al*., 2010]. In order to detect the *P* wave signal through this passband, the BBOBS records were band pass filtered with the corners 0.03 and 0.08 Hz. We then measured relative travel times between two different stations, including the adjacent island stations (open triangles in Figure 1) of the OHP network and the F-net. We also applied the same method to the Russian Far East data. Thus, the data from the northwestern Pacific seafloor include ~1200 first arrival times from the BBOBS array and ~4300 relative travel times from the same BBOBS array.

[4] Traditionally, seismic tomography uses huge data sets of onset times read from short-period seismograms. Theoretically, ray theory is the appropriate method to interpret such data since they represent the minimum travel time. Cross-correlation delays, such as used for differential travel times from broadband seismograms, share the quasi-linearity of onset times but need to be interpreted using finite frequency theory [*Dahlen et al*., 2000; *Mercerat and Nolet*, 2013]. Hybrid inversion, using ray theory for onset times and finite frequency kernels for broadband waveform data, assures compatibility while exploiting different sensitivity [*Monetelli et al*., 2004; *Li et al*., 2008; *Li and van der Hilst*, 2010]. While such a hybrid use of kernels for tomographic inversion is quite reasonable, we calculated the finite frequency kernels for all the data, including the visually picked arrival times and the waveform-correlated differential times by the method of *Dahlen et al*. [2000], in part to assess the appropriateness of such a hybrid approach but also because the presence of noise introduces a frequency dependence to onset data. For the relative time data, we calculated the finite frequency kernels at 0.1 Hz. For the onset time data, we note that the *P* wave onset in the presence of background noise may be regarded as the intersection of the initial *P* wave motion with the noise level. The sensitivity kernel in this case is not restricted to

Table 1. Number of Data, Kernel Type, and Weight for Each Model

	ISC	Handpicked	PP–P	Relative Travel Times
GAP_P2	7.4×10^6 RT 1	5×10^4 RT 1	1.5×10^4 RT 5	NA
Model 1	11.3×10^6 RT 1	6.0×10^4 RT 1	1.5×10^4 RT 5	5.2×10^3 RT 10
Model 2	11.3×10^6 RT 1	6.0×10^4 RT 1	1.5×10^4 FF 5	5.2×10^3 FF 10
Model 3 (GAP_P4)	11.3×10^6 FF 1	6.0×10^4 FF 1	1.5×10^4 FF 5	5.2×10^3 FF 10

RT and FF indicate ray theory and finite frequency, respectively.

the exact raypath and *Stark and Nikolayev* [1993] derived a frequency-dependent kernel instead of the ray theoretical kernel. We calculated the finite frequency kernels for the onset data at 2 Hz. The reason for choosing 2 Hz comes from the result of *Oki et al*. [2004] who measured the S–P differential time by cross-correlating the observed *S* waveform with that synthesized from the observed *P* waveform by taking the physical dispersion into account. They found that this measurement becomes consistent with the handpicked S–P time if we set the reference frequency to 2 Hz in the physical dispersion relation [*Karato*, 1993]. Such consistency implies that the frequencies higher than 2 Hz are invisible or less visible on teleseismic seismograms due partly to the background noise.

[5] We parameterized the whole mantle with blocks of which lateral size varies adaptively according to the kernel density [*Obayashi et al*., 2006, 2009]. The minimum block size is 0.625° × 0.625°, which is comparable to the Fresnel zone width at 2 Hz. We accordingly anticipate only small differences between the inversion results using ray theoretical kernels and using 3-D sensitive kernels when only the short-period ISC onset data are inverted. In order to check this anticipation against our final tomographic model (model 3 named as GAP_P4 of which model parameters are available at http://www.jamstec.go.jp/pacific21/google_earth/klmgenerator/tomography.html), we prepared two trial models. In model 1, ray theory is applied to all the available data. In model 2, finite frequency kernels are applied only to the waveform-based relative time data. Table 1 summarizes the data types, the kernel types, and the weight of the data used for models 1, 2, and 3 as well as the initial model GAP_P2. The variances of all data for models 1 and 3 are smaller than those for GAP_P2 by 1.9% and 6.3%, respectively. The variance reductions are small since GAP_P2 already explain the data well. The variance reduction for model 1 is smaller than model 3. The reduction of the variance for model 1 is limited because all of the data for GAP_P2 including the differential travel times were used based on the same theory (ray theory) for model 1.

3. Results

[6] Because the finite frequency kernel becomes broadest near the bottoming point along a raypath, the transition zone and uppermost lower mantle in our target region (northwestern Pacific) may be imaged differently by the use of either finite frequency kernels or ray theory. Before focusing on the northwestern Pacific where finite frequency kernels play an important part, we look at global features of subducting slabs above and below the 660 km discontinuity. Figure 2 shows *P* wave velocity perturbations of model 3 at the depths of about 500 km and 950 km. There are laterally extended fast anomalies at both depths along the Circum Pacific subduction zones that correspond to the slabs stagnant in the lowermost upper mantle and the uppermost lower mantle [*Fukao et al*., 2001]. In these regions, the stagnant slabs in the lowermost upper mantle and those in the uppermost lower mantle are closely adjacent to each other with little overlap, suggesting that they represent processes before and after the slab penetration, respectively. Further discussions about the reservoirs of slabs above and below the 660 km discontinuity are made in *Fukao and Obayashi* [2013].

[7] Figure 3 shows *P* wave velocity perturbations of the initial model GAP_P2, model 1, and model 3 at the depths around 600 km and 670 km, respectively. The differences of models 1 and 3 from GAP_P2 are shown in Figure S1 in the supporting information. The difference between GAP_P2 and model 1 reflects the addition of new data. In particular, extensive fast anomalies have appeared underneath the central Philippine Sea mainly by addition of the BBOBS data. The difference between models 1 and 3 is the consequence of application of finite frequency kernels. Figure S2 in the supporting information shows a comparison of kernel densities among GAP_P2, model 1, and model 3. Here a kernel density is defined as the sum (ray theoretical case) or volume integral (finite frequency case) of kernels within a block of equal size. This comparison demonstrates that the differences of tomographic images between model 3 and GAP_P2 (or model 1) beneath the Philippine Sea are

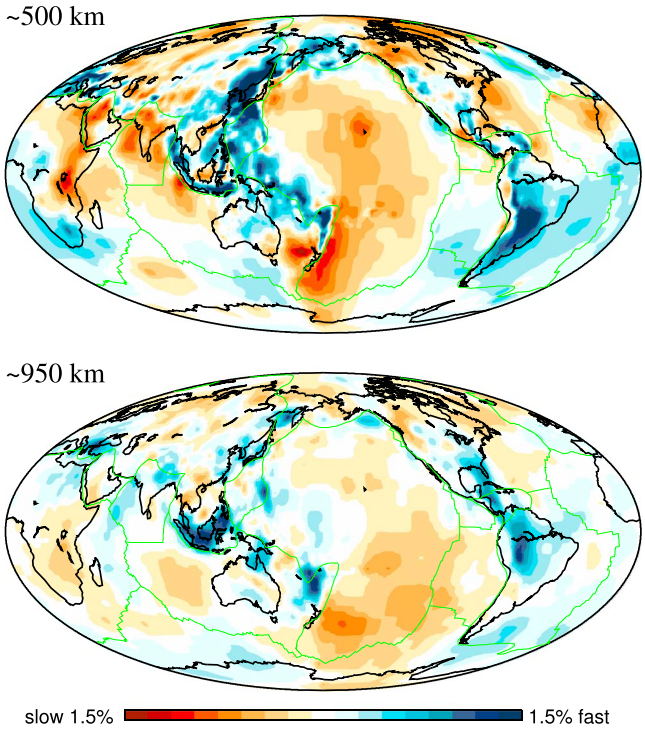

Figure 2. Global maps of *P* wave velocity anomalies of the GAP_P4 (model 3) at depths about 500 km and 950 km.

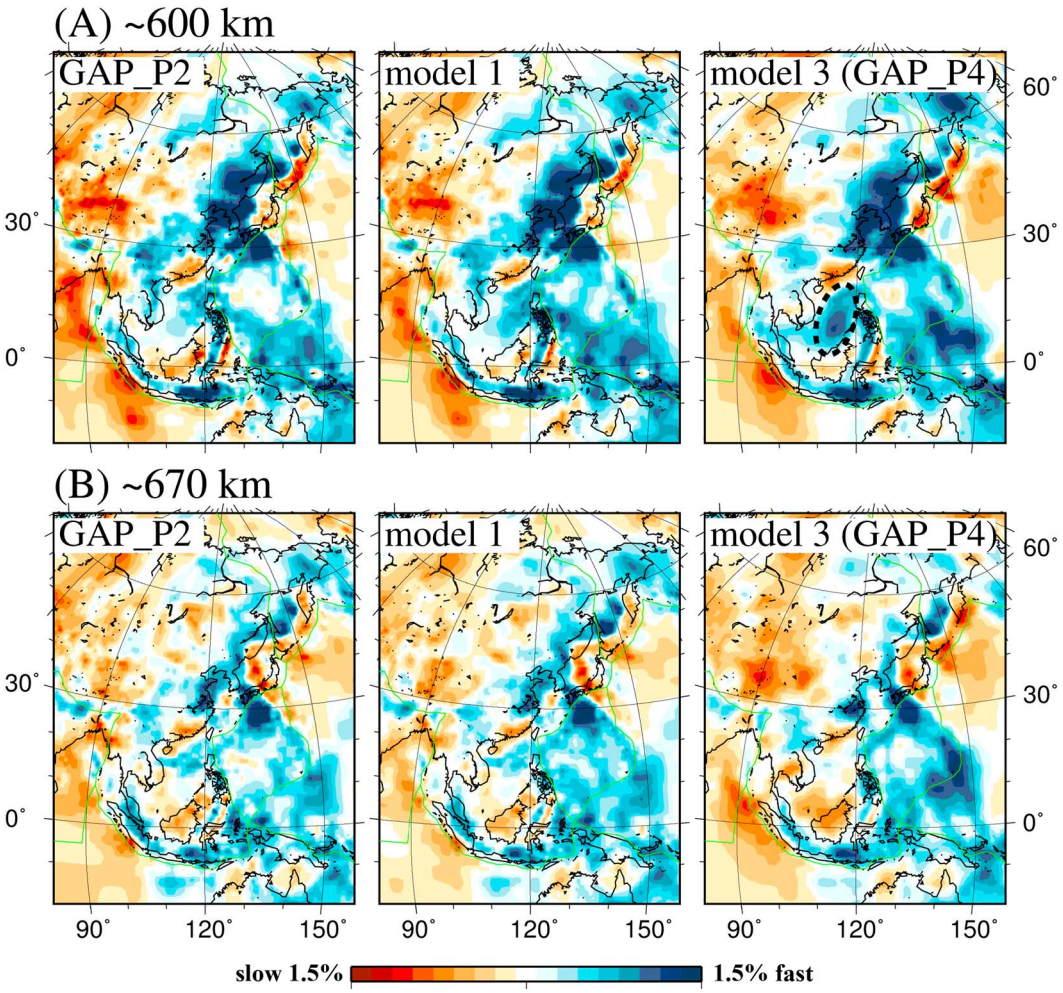

Figure 3. *P* wave velocity anomalies of the initial model GAP_P2, model 1, and GAP_P4 (model 3) at depths about (a) 600 km and (b) 670 km in the region of the northeastern Pacific. The slab beneath South China Sea in the transition zone is shown by dotted line.

due largely to whether or not finite frequency kernels are used for waveform-based data. Although model 2 is not shown here, comparison of models 2 and 3 indicates that the use of finite frequency kernels is of limited significance for the onset data but has significant impact on the cross-correlated relative travel time data. The differences between model 3 and GAP_P2 are larger than those between model 1 and GAP_P2 (Figure S1). Such differences are caused by finite frequency kernels for the relative travel time data. Model 1 is similar to GAP_P2 despite the increase of the onset data, suggesting that the additional onset data are almost consistent with GAP_P2 when we use ray theoretical kernel for it. Note, for example, that although the image of slab subducting eastward beneath Molucca in model 3 seems to be more similar to that in GAP_P2 than that in model 1, the difference of model 3 from GAP_P2 is much larger than that of model 1 from GAP_P2 even in such a region.

[8] The use of finite frequency kernels (model 3) has enabled us to clarify a high-velocity stagnant slab isolated in the transition zone under the South China Sea. The similar image is also seen in some *P* wave tomography models [e.g., *Lallemand et al*., 2001; *Simmons et al*., 2012]. According to *Lallemand et al*. [2001], this image is sharply truncated at a latitude of 20°N, to the north of which the slab of the South China Sea lithosphere of the Eurasian plate subducted from the Manila Trench is clearly imaged. The stagnant slab beneath the South China Sea may be associated with the subduction of the Philippine Sea plate, paleo-Philippine Sea plate, or the former subduction of the Pacific plate [*Maruyama et al*., 1997; *Hall*, 2002; *Yin*, 2010]. Similarly, the use of finite frequency kernels has enabled us to sharpen the image of the Pacific slab subducted from the Mariana trench. Figure 4 shows this situation in a cross-sectional view along the profile shown in Figure 1. As compared to model 1, model 3 images more clearly the downgoing slab that penetrates the 660 km discontinuity and begins to be trapped in the uppermost lower mantle. We evaluate the effect of depression of the 660 km discontinuity due to the cold Mariana slab by introducing a slower-than-normal block with a lateral size of 1.25° and a thickness of 83 km across the 660 km discontinuity. As detailed in the supplementary text along with Figure S3, the test result shows that the effect of the 660 km depression is minor. Model 3 at the same time images more sharply the stagnant slab above the 660 km discontinuity that is apparently detached from the penetrating slab [*Fukao and Obayashi*, 2013]. This stagnant slab image extends southward across the southernmost end of the Mariana trench and bends to the east to extend beneath the Caroline Ridge. Besides the slabs

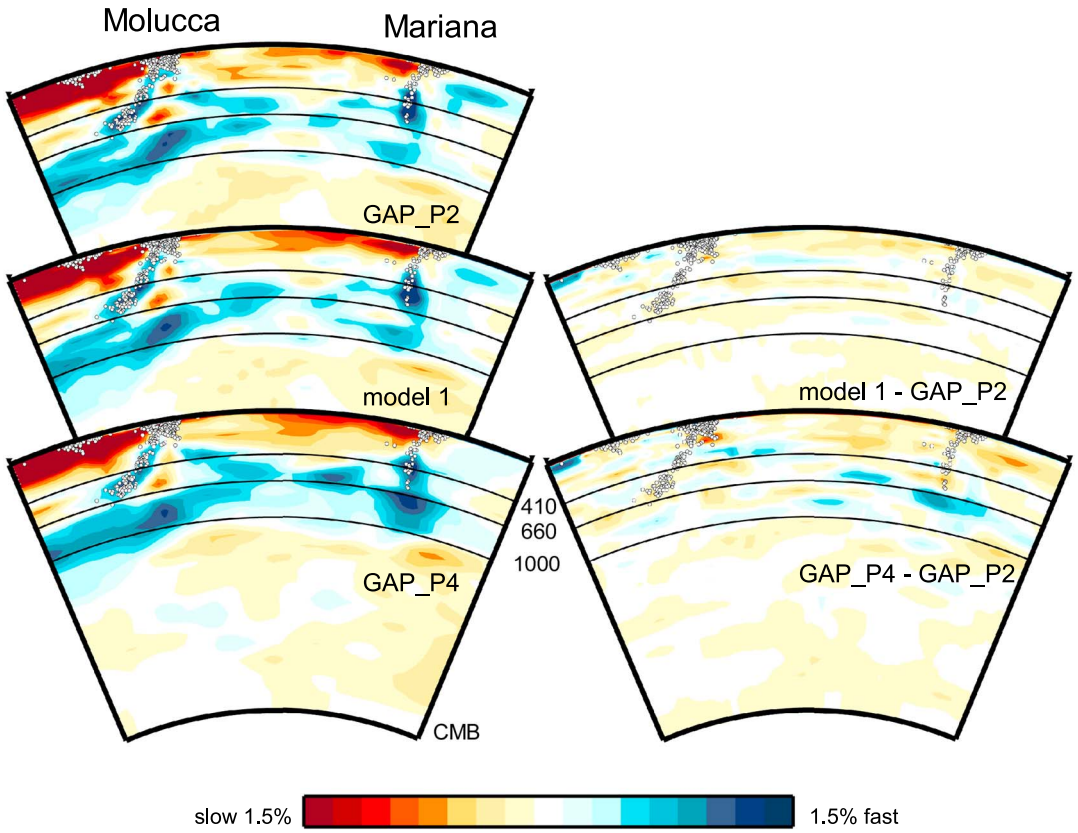

Figure 4. Cross sections of the GAP_P2, model 1, and the GAP_P4 (model 3) along the great circle path indicated in Figure 1. Differences of model 1 and GAP_P4 from GAP_P2 are shown in the right column. The open circles indicate earthquakes with magnitudes mb > 4.0.

described above, the slab of the Molucca Sea plate that subducts to the east beneath the Halmahera arc [*Widiyantoro and van der Hilst*, 1997; *Hall and Spakman*, 2002] to reach the 660 km discontinuity is clearly imaged, although *Hall and Spakman* [2002] emphasized the continuation of Halemahera slab to the trapped slab in the uppermost lower mantle.

[9] Figures 3 and 4 indicate that model 1 is more similar to GAP_P2 than model 3 even though models 1 and 3 use the same data set. This implies that the location and intensity of slab-related fast anomalies depend strongly on whether the kernels are calculated based on the ray or finite frequency theory if the waveform-based data have a significant proportion of the raypath coverage in the targeted region (Figure S2 in the supporting information). This also implies that broadband seismic observations in the area of sparse station distribution play a more important role to improve target images than expected from simple raypath coverage arguments. Although we found little differences between models 2 and 3 in the essential features, model 3 gives in general a smoother anomaly pattern than model 2, because block representation of 2 Hz kernels is still a spatially smoother function than that of ray theoretical kernels.

4. Summary

[10] Our previous *P* wave velocity model GAP_P2 is based on about 7 million ISC data, a limited number of broadband data, and employment of classical ray theoretical kernels. Model GAP_P4 is the consequences of an increase in ISC data, an extensive addition of broadband data, including the manually picked first arrival onset data and differential travel time data measured using a cross-correlation method at around 0.1 Hz, and an application of the finite frequency kernels to all the available data. As demonstrated in Figures 3 and 4, the differences between the two models are significant especially in the transition zone and uppermost lower mantle beneath the South China Sea, the southern Philippine Sea including the Mariana trench, and the Caroline Ridge region. In order to examine the finite frequency effect on these differences, we tested three models (Table 1) which share the same enhanced set of travel time data. Model 1 employs the classical ray theoretical kernels for all the data. Model 2 employs the finite frequency kernels only for broadband differential travel time data, and model 3 is GAP_P4 that employs the finite frequency kernels for all the available data. Differences between GAP_P2 and model 1 are not so large in spite of a significant expansion of the data set in model 1. Differences between models 2 and 3 are in general very small as might be expected from the comparativeness of 2 Hz Fresnel zone width with the minimum block size in model space, although model 3 gives somewhat smoother images of slab anomalies (Figure 3). Significant difference occurs between model 1 and models 2 and 3, depending on whether the ray kernels or finite frequency kernels are applied to the data retrieved mainly from the BBOBSs. BBOBS observations in regions of poor station coverage should be more useful to sharpen images of subducted slabs beneath ocean floors than expected from simple raypath coverage arguments.

[11] **Acknowledgments.** We thank F. Niu and an anonymous reviewer for critical and constructive reviews. This study was supported by Japanese grants-in-aid for Science Research in the Priority Areas of "Stagnant Slab: A New Keyword for Mantle Dynamics" (16075208), JSPS Excellent Young Researchers Overseas Visit Program and ERC Advanced grant 226837.

[12] The Editor thanks Fenglin Niu and an anonymous reviewer for their assistance in evaluating this paper.

References

Bijwaard, H., W. Spakman, and E. R. Engdahl (1998), Closing the gap between regional and global travel time tomography, *J. Geophys. Res.*, *103*, 30,055–30,078.

Boschi, L., and A. M. Dziewonski (1999), High- and low-resolution images of the Earth's mantle: Implications of different approaches to tomographic modeling, *J. Geophys. Res.*, *104*, 25,567–25,594.

Dahlen, F. A., S. H. Hung, and G. Nolet (2000), Frechet kernels for finite-frequency traveltimes—I. Theory, *Geophys. J. Int.*, *141*, 157–174.

Fukao, Y., and M. Obayashi (2013), Subducted slabs stagnant above, penetrating through and trapped below the 660-km discontinuity, *J. Geophys. Res. Solid Earth*, doi:10.1002/2013JB010466.

Fukao, Y., M. Obayashi, H. Inoue, and M. Nenbai (1992), Subducting slabs stagnant in the mantle transition zone, *J. Geophys. Res.*, *97*, 4809–4822.

Fukao, Y., S. Widiyantoro, and M. Obayashi (2001), Stagnant slabs in the upper and lower mantle transition region, *Rev. Geophys.*, *39*, 291–323.

Fukao, Y., M. Obayashi, T. Nakakuki, and the Deep Slab Project group (2009), Stagnant slab: a review, *Annual Rev. Earth Plane. Sci.*, *37*, 19–46.

Hall, R. (2002), Cenozoic geological and plate tectonic evolution of SE Asia and the SW Pacific: Computer-based reconstructions, model and animations, *J. Asian Earth Sci.*, *20*, 353–431.

Hall, R., and W. Spakman (2002), Subducted slabs beneath the eastern Indonesia-Tonga region: Insights from tomography, *Earth Planet. Sci. Lett.*, *201*, 321–336.

Hung, S. H., F. A. Dahlen, and G. Nolet (2000), Frechet kernels for finite-frequency traveltimes—II. Examples, *Geophys. J. Int.*, *141*, 175–203.

Hung, S.-H., W.-P. Chen, and L.-Y. Chiao (2011), A data-adaptive, multiscale approach of finite-frequency, traveltime tomography with special reference to P and S wave data from central Tibet, *J. Geophys. Res.*, *116*, B06307, doi:10.1029/2010JB008190.

Isse, T., et al. (2009), Seismic structure of the upper mantle beneath the Philippine Sea from seafloor and land observation: Implications for mantle convection and magma genesis in the Izu-Bonin-Mariana subduction zone, *Earth Planet. Sci. Lett.*, *278*, 107–119.

Isse, T., H. Shiobara, J. P. Montagner, H. Sugioka, A. Ito, A. Shito, T. Kanazawa, and K. Yoshizawa (2010), Anisotropic structures of the upper mantle beneath the northern Philippine Sea region from Rayleigh and Love wave tomography, *Phys. Earth Planet. Int.*, *183*, 33–43.

Karato, S. (1993), Importance of anelasticity in the interpretation of seiic tomography, *Geophys. Res. Lett.*, *20*, 1623–1626.

Kennett, B. L. N., S. Widiyantoro, and R. D. van der Hilst (1998), Joint seismic tomography for bulk sound and shear wave speed in the Earth's mantle, *J. Geophys. Res.*, *103*, 12,469–12,493.

Lallemand, S., Y. Font, H. Bijwaard, and H. Kao (2001), New insights on 3-D plates interaction near Taiwan from tomography and tectonic implications, *Tectonophysics*, *335*, 229–253.

Li, C., and R. D. van der Hilst (2010), Structure of the upper mantle and transition zone beneath Southeast Asia from traveltime tomography, *J. Geophys. Res.*, *115*, B07308, doi:10.1029/2009JB006882.

Li, C., R. D. van der Hilst, E. R. Engdahl, and S. Burdick (2008), A new global model for P wave speed variations in Earth's mantle, *Geochem. Geophys. Geosys.*, *9*, Q05018, doi:10.1029/2007GC001806.

Liu, Q., and J. Tromp (2008), Finite-frequency sensitivity kernels for global seismic wave propagation based upon adjoint methods, *Geophys. J. Int.*, *174*, 265–286.

Maruyama, S., Y. Isozaki, G. Kimura, and M. Terabayashi (1997), Paleogeographic maps of the Japanese Islands: Plate tectonic synthesis from 750 Ma to the present, *Island Arc*, *6*, 121–142.

Mercerat, E. D., and G. Nolet (2013), On the linearity of cross-correlation delay times in finite-frequency tomography, *Geophys. J. Int.*, *192*, 681–687.

Miyamachi, H., et al. (2009), Construction of the broadband seismic network in Far Eastern Russia for imaging the stagnant slab, *Geophys. Bull. Hokkaido Univ.*, *72*, 37–49 (in Japanese with English abstract).

Monetelli, R., G. Nolet, F. A. Dahlen, G. Masters, E. R. Engdahl, and S.-H. Hung (2004), Finite-frequency tomography reveals a variety of plumes in the mantle, *Science*, *303*, 338–343.

Obayashi, M., D. Suetsugu, and Y. Fukao (2004), PP-P differential traveltime measurement with crustal correction, *Geophys. J. Int.*, *157*, 1152–1162.

Obayashi, M., H. Sugioka, J. Yoshimitsu, and Y. Fukao (2006), High temperature anomalies oceanward of subducting slabs at the 410-km discontinuity, *Earth Planet. Sci. Lett.*, *243*, 149–158.

Obayashi, M., J. Yoshimitsu, and Y. Fukao (2009), Tearing of stagnant slab, *Science*, *324*, 1173–1175.

Okada, Y., K. Kasahara, S. Hori, K. Obara, S. Sekiguchi, H. Fujiwara, and A. Yamamoto (2004), Recent progress of seismic observation networks in Japan—Hi-net, F-net, K-NET and KiK-net, *Earth Planets Space*, *56*, 15–28.

Oki, S., Y. Fukao, and M. Obayashi (2004), Reference frequency of teleseismic body waves, *J. Geophys. Res.*, *109*, B04304, doi:10.1029/2003JB002821.

Shiobara, H., K. Baba, H. Utada, and Y. Fukao (2009), Ocean bottom array probes stagnant slab beneath the Philippine Sea, *Eos Trans. AGU*, *90*(9), 70–71.

Sigloch, K. (2011), Mantle provinces under North America from multi-frequency P wave tomography, *Geochem. Geophys. Geosyst.*, *12*, Q02W08, doi:10.1029/2010GC003421.

Sigloch, K., and M. G. Mihalynuk (2013), Intra-oceanic subduction shaped the assembly of Cordilleran North America, *Nature*, *496*, 50–56.

Sigloch, K., N. McQuarrie, and G. Nolet (2008), Two-stage subduction history under North America inferred from multiple-frequency tomography, *Nat. Geosci.*, *1*, 458–462.

Simmons, N. A., S. C. Myers, G. Johannesson, and E. Matzel (2012), LLNL-G3Dv3: Global P wave tomography model for improved regional and teleseismic travel time prediction, *J. Geophys. Res.*, *117*, B10302, doi:10.1029/2012JB009525.

Stark, P. B., and D. I. Nikolayev (1993), Toward tubular tomography, *J. Geophys. Res.*, *98*, 8095–8106.

Suetsugu, D., et al. (2010), Depths of the 410-km and 660-km discontinuities in and around the stagnant slab beneath the Philippine Sea: Is water stored in the stagnant slab?, *Phys. Earth Planet. Int.*, *183*, 270–279.

Sugioka, H., Y. Fukao, and T. Kanazawa (2010), Evidence for infragravity wave-tide resonance in deep oceans, *Nat. Commun.*, *1*, 84, doi:10.1038/ncomms1083.

Tanaka, S., M. Obayashi, D. Suetsugu, H. Shiobara, H. Sugioka, J. Yoshimitsu, T. Kanazawa, Y. Fukao, and G. Barruol (2009), P-wave tomography of the mantle beneath the South Pacific Superswell revealed by joint ocean floor and islands broadband seismic experiments, *Phys. Earth Planet. Int.*, *172*, 268–277.

Toomey, D. R., W. S. D. Wilcock, S. C. Solomon, W. C. Hammond, and J. A. Orcutt (1998), Mantle seismic structure beneath the MELT region of the East Pacific Rise from P and S wave tomography, *Science*, *280*, 1224–1227.

van der Hilst, R., R. Engdahl, W. Spakman, and G. Nolet (1991), Tomographic imaging of subducted lithosphere below northwest Pacific island arcs, *Nature*, *353*, 37–43.

van der Hilst, R. D., S. Widiyantoro, and E. R. Engdahl (1997), Evidence for deep mantle circulation from global tomography, *Nature*, *386*, 578–584, doi:10.1038/386578a0.

Webb, S. C. (1998), Broadband seismology and noise under the ocean, *Rev. Geophys.*, *36*, 105–142.

Widiyantoro, S., and R. van der Hilst (1997), Mantle structure beneath Indonesia inferred from high-resolution tomographic imaging, *Geophys. J. Int.*, *130*, 167–182.

Yin, A. (2010), Cenozoic tectonic evolution of Asia: A preliminary synthesis, *Tectonophysics*, *488*, 293–325.